Remote Sensing Detection of atmospheric pollutants using Lidar, Sodar and correlation with air quality data in an industrial area

Juliana Steffens[a], Renata F. da Costa[b], Eduardo Landulfo[b], Roberto Guardani[a], Paulo F.Moreira Junior[a], Gerhard Held[c]
[a]Escola Politécnica da Universidade de São Paulo, Avenida Gualberto 2345, São Paulo, Brazil, 05508-970
[b]Instituto de Pesquisas Energéticas e Nucleares, Avenida Prof. Lineu Prestes 2242, São Paulo, Brazil, 05508-000
[c]Instituto de Pesquisas Meteorológicas - IPMet-UNESP, Av. Luis Edmundo Carrijo Coube, Bauru, São Paulo, Brazil, 17033-360

ABSTRACT

Optical remote sensing techniques have obvious advantages for monitoring gas and aerosol emissions, since they enable the operation over large distances, far from hostile environments, and fast processing of the measured signal. In this study two remote sensing devices, namely a Lidar (Light Detection and Ranging) for monitoring the vertical profile of backscattered light intensity, and a Sodar (Acoustic Radar, Sound Detection and Ranging) for monitoring the vertical profile of the wind vector were operated during specific periods. The acquired data were processed and compared with data of air quality obtained from ground level monitoring stations, in order to verify the possibility of using the remote sensing techniques to monitor industrial emissions. The campaigns were carried out in the area of the Environmental Research Center (Cepema) of the University of São Paulo, in the city of Cubatão, Brazil, a large industrial site, where numerous different industries are located, including an oil refinery, a steel plant, as well as fertilizer, cement and chemical/petrochemical plants. The local environmental problems caused by the industrial activities are aggravated by the climate and topography of the site, unfavorable to pollutant dispersion. Results of a campaign are presented for a 24-hour period, showing data of a Lidar, an air quality monitoring station and a Sodar.

Keywords: Lidar technique, Sodar, vertical profiles of Lidar & Sodar observations, air quality.

1. INTRODUCTION

The increased awareness of the environmental impact of certain industrial activities, as well as more stringent regulations of emissions, call for more powerful measurement techniques for air pollution monitoring**.** The amount and composition of the anthropogenic hydrocarbons emissions from sources, such as petrochemical industries, pipelines, road transportation, use of solvents and biomass burning, are also crucial for understanding their impact on the atmospheric chemistry on regional and global effects [1]. In this context, laser remote sensing techniques have been applied to a variety of environmental measurement tasks for several decades, but the problems of remote recognition of aerosol impurities in the atmosphere remained unattended. At the same time, the urgency of these problems is evident, as solving them is necessary for the realization of monitoring the atmosphere near dangerous industries [2].

Laser remote sensing techniques are all a form of laser radar (Lidar) systems, and are gaining high acceptance as long-range, non-invading spectroscopic probes of the chemical composition and proprieties of the atmosphere. Through its high temporal and spatial resolution, the Lidar technique is a powerful tool for real-time visualization [3]. It can provide a wide spectrum of information, which contributes significantly towards a better understanding of various phenomena occurring in the atmosphere, like pollution emission, its transformation and migration, inversion layer formation, cloud physics and chemistry, etc. Such information is useful for many branches of science, from physics of the atmosphere and the Earth sciences to the interaction of aerosol particles on living organisms[4]. Particular attention has been given to the influence of aerosol particles on human health and its dependence on their sizes and chemical composition [5]. In this context, the town of Cubatão in Brazil has many problems with air quality. The city is one of the largest industrial sites

Lidar Technologies, Techniques, and Measurements for Atmospheric Remote Sensing VII, edited by Upendra N. Singh, Gelsomina Pappalardo, Proc. of SPIE Vol. 8182, 81820Z

in the country. Within an area of ca. 40 km^2, there are 23 large industries, including a steel plant, an oil refinery, 7 fertilizer plants, a cement plant, and 11 chemical/petrochemical plants, adding up to 260 emission sources of pollutants, besides the urban area, with ca 130 thousand inhabitants. A number of initiatives adopted since the 80´s have led to significant reductions in industrial emissions. However, the environmental problems caused by the industrial activities are aggravated by the climate and topography of the site, unfavorable to pollutant dispersion.

In a partnership with the University of São Paulo (USP), the Brazilian oil company PETROBRAS has supported the installation of an Environmental Research Center - CEPEMA- located in the industrial site, where a Lidar system at 355, 532 and 1064 nm wavelength, as well as a Sodar/RASS system and a air quality monitoring station were deployed to characterize the vertical profile of the atmosphere.

1.1. Description of the Cubatão Region

Cubatão occupies the southeastern portion of the state of São Paulo, being bordered in the north by the Serra do Mar mountain range and on the south by the cities of São Vicente and Santos on the Atlantic Ocean (Fig.1). Cubatão presents distinct meteorological characteristics relative to the other areas in this region. The surface wind velocities from the north-northeast during the day are influenced by local topography with hills and crystalline elevations between 200 and 1000 m intercalated by flat low lying ocean inlets[6]. Because of its location, the wind and thus the conditions for the dispersion of pollutants within the Cubatão area are strongly influenced by local topography. The climate is tropical and cloudy with no dry season and shows relatively high annual averages for temperature (23°C) and precipitation (2600 mm). The large variation in rainfall in the region is controlled by the movements of sea-land and mountain-valley winds, which influence the mesoscale diurnal variation of precipitation over Cubatão through the convergence of sea breezes. Wind behavior in the area is characterized by drainage wind, which begins at dusk or even before and is favored by the slopes to the north-northwest, which are heated during the day. This is particularly important for synoptic-scale anticyclonic situations with clear skies, when the air changes in the area are practically dominated by meso- and micrometeorological phenomena[7]. Strong local-scale drainage winds from the northeast transport industrial emissions in the direction of the urban area (Fig. 1). Observations show that the stable air mass, with most emissions from fertilizer industries, moves from the base of the mountains to the urban area of Cubatão. Solar heating of the slopes results in the development of anabatic winds and sea breezes, which are easily viewed by the trajectory of the plumes from chimneys. These winds are generally associated with high aerosol concentrations. During winter mornings, layers of surface temperature inversions of different thicknesses and different intensities are observed.

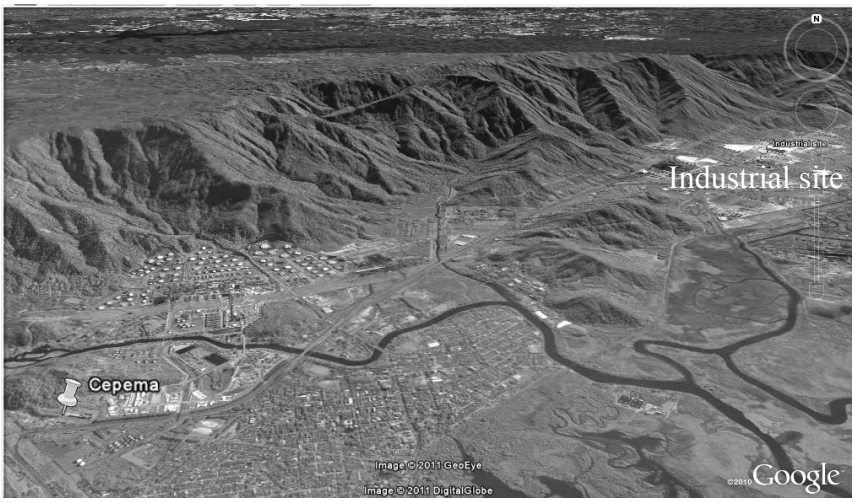

Figure 1- Map of Cubatão city and the monitoring site at Cepema relative to the Industrial Site and the Serra do Mar mountain range.

1.2- Lidar and Sodar/RASS

Lidar (an acronym for light detection and ranging) is a remote sensing technique used predominately for measuring atmospheric parameters, such as temperature, atmospheric composition and wind. Lidar operates on the same principle

as radar; in fact, it is sometimes called laser-radar. Both techniques transmit a beam of pulsed electromagnetic radiation and subsequently detect any radiation scattered back to the instrument, which then is analyzed in order to determine some property or properties of the medium through which the radiation traveled. However, Lidar and radar differ in the wavelength of the radiation utilized. Lidar uses light in the ultraviolet, visible and infrared, which in modern Lidar systems is generated by lasers. The range of atmospheric parameters measurable with Lidar includes temperature, wind velocity, atomic and molecular species concentration, and aerosol and cloud properties. In addition to its atmospheric applications, Lidar is also used in ocean research and military applications, including the detection of chemical and biological agents and the remote identification and tracking of vehicles. Lidar-equipped binoculars are used by hunters and golfers as they provide accurate range measurements[8].

The Sodar operates by emitting a short pulse and listening to the atmospheric echo from that pulse. The echo is a result of the continuous interaction between the outward propagating acoustic energy and atmospheric turbulence. The echo, when received by the Sodar microphone array, is processed for its frequency content. A change in frequency is associated with movement of the atmospheric turbulence by the local wind field. Using the Doppler shift principles, the echo frequency will be greater than the pulse frequency if this movement is toward the microphone array. A lower frequency with respect to the pulse frequency implies that the movement is away from the microphone array. The outgoing pulse is not affected in frequency until it is echoed by the interaction with atmospheric turbulence and retuned to the microphones. The time this process takes is proportional to the distance (height). Using information from three different directions (and decoding the data in terms of its first order geometry (i.e., neglecting refraction effects), the altitude gated frequencies enable a full wind profile to be measured [9, 10].

A radio acoustic sounding system (RASS) is a system for measuring the atmospheric lapse rate, using backscattering of radio waves from an acoustic wave front to measure the speed of sound at various heights above the ground. This is possible because the compression and rarefaction of air by an acoustic wave changes the dielectric properties, producing partial reflection of the transmitted radar signal. From the speed of sound, the temperature of the air in the planetary boundary layer can be computed. The maximum altitude range of RASS systems is typically 750 meters, although observations have been reported up to 1.2 km in moist air [11,12].

2. MATERIALS AND METHODS

The Lidar system, Sodar and air quality monitoring station are operated in the CEPEMA (Environmental Research Center) of the University of São Paulo, situated on the northwestern outskirts of Cubatão's urban area. The Lidar observations, consisting of amplitude of backscattered light, were compared with the air quality measurements and Sodar data.

2.1- Lidar

The Lidar backscattered light signal at different altitudes was corrected for distance and air mass. Thus, the raw Lidar signal was converted into scattering ratio (ratio of the total aerosol plus molecular backscattering to the molecular backscattering). The main characteristics of the Lidar System are shown in Table 1.

Table 1- Multi-wavelenght elastic Lidar system.

Laser	
Laser type	Nd:YAG Laser (ICE 450/CFR)
Wavelenght	355, 532, 1064 nm
Pulse energy	100 mJ (at 355 nm), 200 mJ (at 532 nm) and 400 mJ (at 1064 nm)
Repetition rate	20 Hz
Pulse duration	(7 ± 2) ns
Reciever optics	
Optical design	150 mm diameter cassegranian telescope
Focal Length	1000 mm
Field of view	1mrad
Transient Recorder	Licel (TR 20-80) 10-250 MHz bandwidth

2.2 Sodar

A Sodar with RASS is deployed for monitoring the vertical distribution of wind (u, v, w) and temperature within the lower Planetary Boundary Layer (PBL). The nominal height of the Sodar is up to 2000 m and of the RASS ca 1000 m AGL, depending on settings and meteorological conditions. Unfortunately, due to limitations of the current location, not being ideal, the Sodar only reaches up to about 500 m AGL.

2.3- Data Collection

Simultaneous observations from Lidar, Sodar and an air quality monitoring station in Cubatão during the 24-hour period from May 25th , 10:00 to May 26th , 10:00, 2011 are presented.

2.4- Data Analyses

From the above 24-hour period, pre-review periods without clouds and with greater presence of mass volume were selected from 17:30 until 23:36, because it is the period that had an entry of mass at a height near 800m, as shown in Figure 2-4. This period was divided into 9 intervals and the data recorded by the Lidar in these intervals were summed to determine the backscatter coefficient and the color ratio. Table 2 shows the ranges of measurement for each vertical profile analysis.

Table 2- Ranges of measurement for each vertical profile analysis

Lidar data selection	
Vertical Profile	Measurement interval
VP1	17:30 – 17:59
VP2	18:00 – 18:29
VP3	18:30 – 18:59
VP4	19:00 – 19:29
VP5	19:30 – 19:59
VP6	21:42 – 22:12
VP7	22:13 – 22:42
VP8	22:43 – 23:13
VP9	23:14 – 23:36

The aerosol backscatter coefficient, $\beta^{aer}(\lambda_L, r)$, can be evaluated from the aerosol scattering ratio as follows:

$$\beta^{aer}(\lambda_L, r) = \beta_{\pi}^{mol}(\lambda_L, r)\left(SR(\lambda_L, r) - 1\right) \tag{1}$$

where $\beta_{\pi}^{mol}(\lambda_L, r)$ is the Rayleigh backscatter coefficient at the laser wavelength calculated using a standard atmospheric densities. The aerosol scattering ratio, $SR(\lambda_L, r)$, is defined as the ratio of the total (molecular and particle) backscatter coefficient divided by the molecular backscatter coefficient[13].

The backscatter coefficient color ratio was defined as follows:

$$\chi = \frac{\beta^{aer}(\lambda_{L1}, r)}{\beta^{aer}(\lambda_{L2}, r)} \tag{2}$$

where λ_{L1} is a wavelength higher than λ_{L2} . The backscatter color ratio is inversely related to aerosol size and identifies the biggest aerosols associated with smoke and urban pollution[14].

3. RESULTS

Figures 2 to 4 show a time series of the vertical profile backscatter Lidar signal at 355 nm, 532 nm and 1064 nm. The time series span over 24 hours continuously. A vertical profile is recorded in 60 seconds (averaging 1200 Lidar measurements). The intensity scale in the Figures is related to the efficiency of answer by the photomultipliers (PMT) and the photodiode (APD).

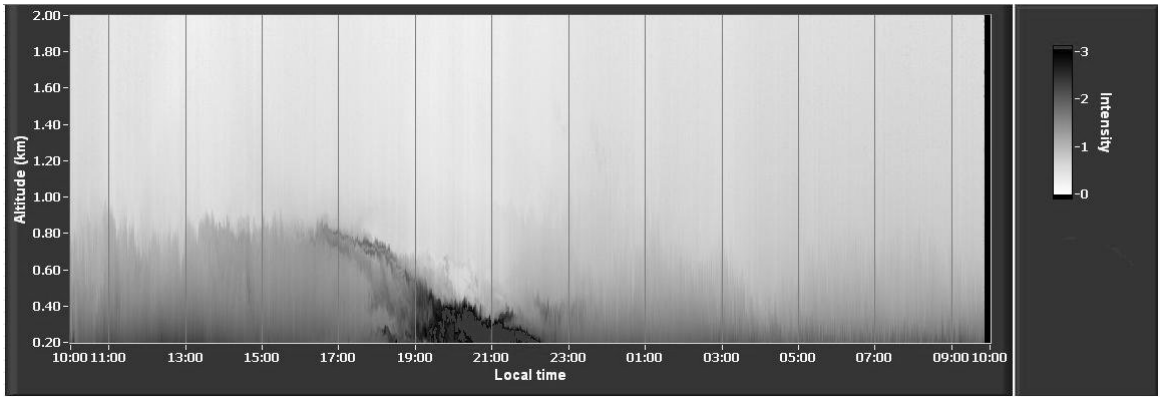

Figure 2- Vertical Backscatter Lidar signal at 355 nm.

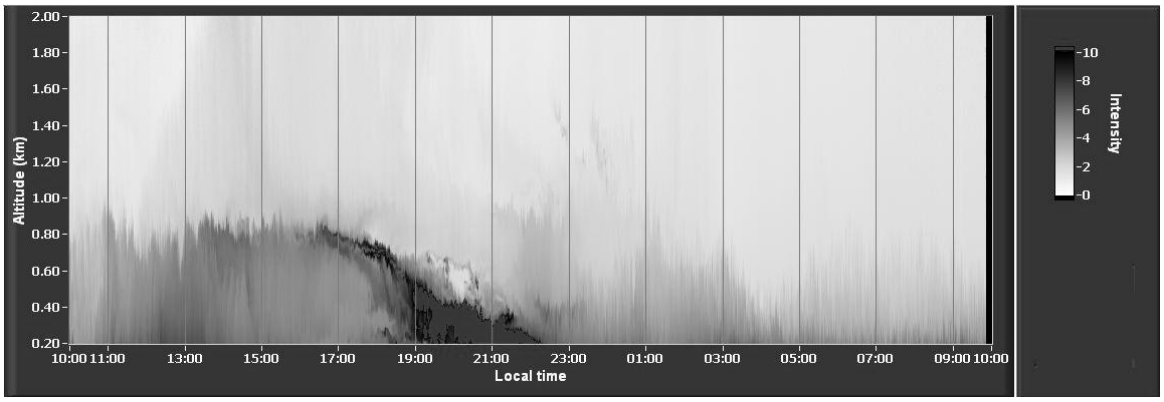

Figure 3- Vertical Backscatter Lidar signal at 532 nm

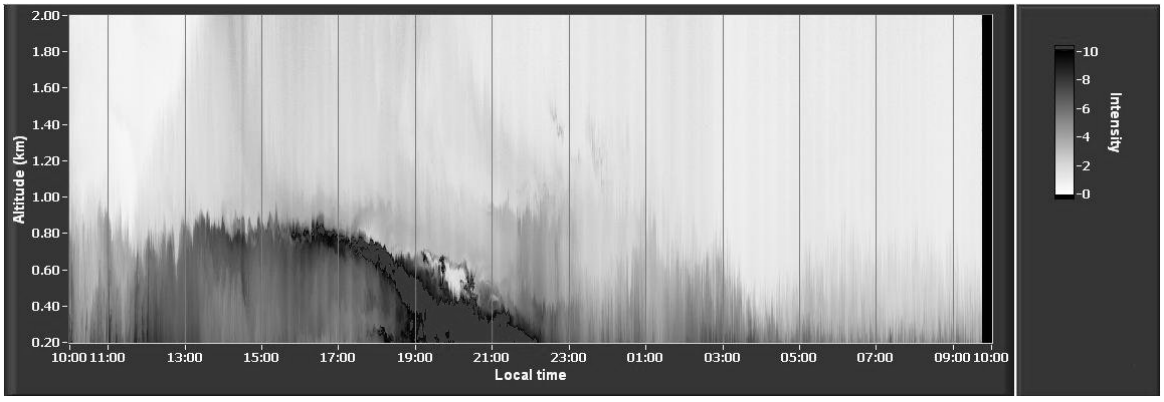

Figure 4 - Vertical Backscatter Lidar signal at 1064 nm.

Figures 5 and 6 show the vertical profiles of the backscatter coefficient and the color ratio, respectively. It is possible to see that the value of the backscatter coefficient for 355 nm is about three orders of magnitude higher than that of 1064 nm. This can be explained by the fact that the Rayleigh scattering intensity is inversely proportional to the forth power of the wavelength of the incident radiation. The VP5 shows the highest values for the backscattering coefficient at all wavelengths and compared to Figures 2 to 4 it is possible to observe that during this period a massive inflow is identified by the value of the intensity of the corrected signal. However, the VP6, VP7 and VP8 profiles have the lowest values of the backscatter coefficient, indicating the presence of a relatively clean atmosphere at these intervals.

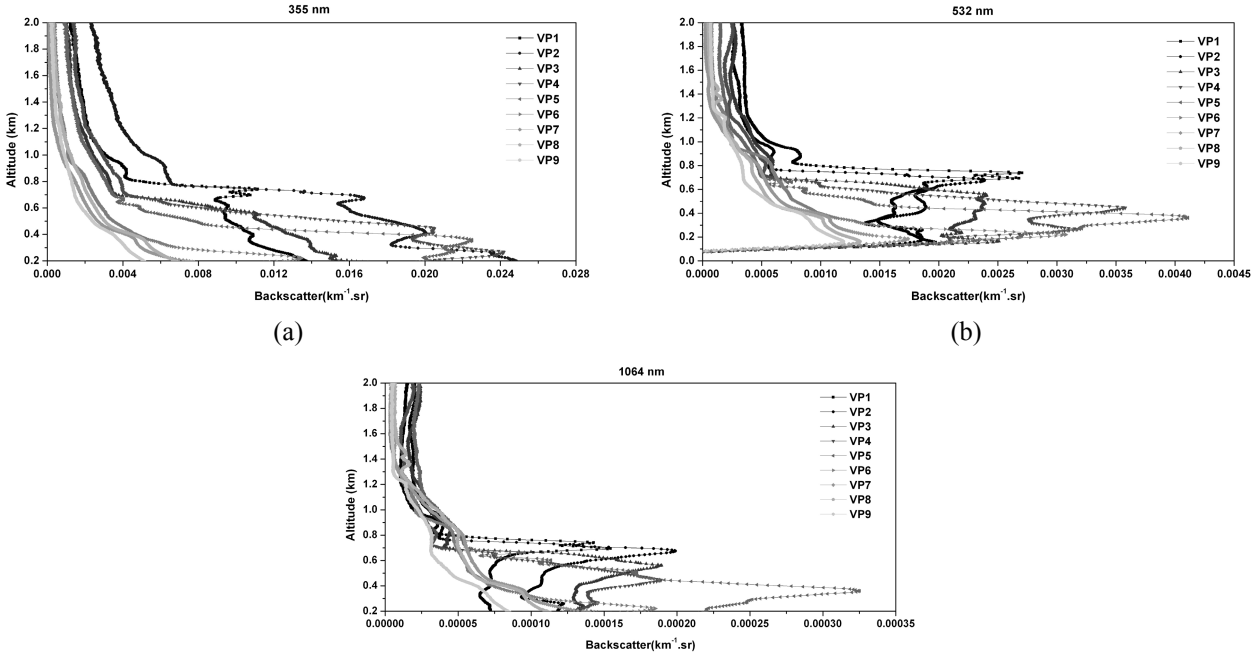

(a) (b)

(c)

Figure 5 - Vertical profile backscatter coefficient: (a) 355 nm; (b) 532 nm; (c) 1064 nm.

The profiles VP6, VP7 and VP8 present the highest values for the three color ratios calculated, which may indicate that the greater the color ratio, the smaller the particulate material, showing that, in fact the color ratio is inversely proportional to particulate size.

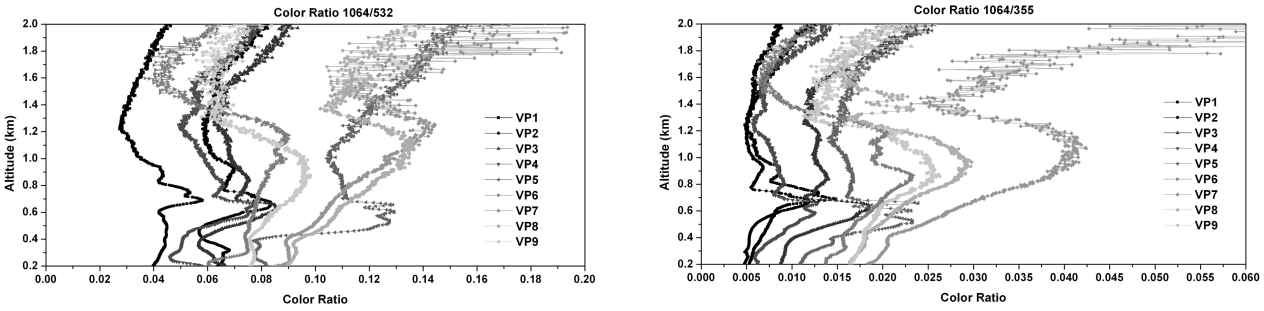

(a) (b)

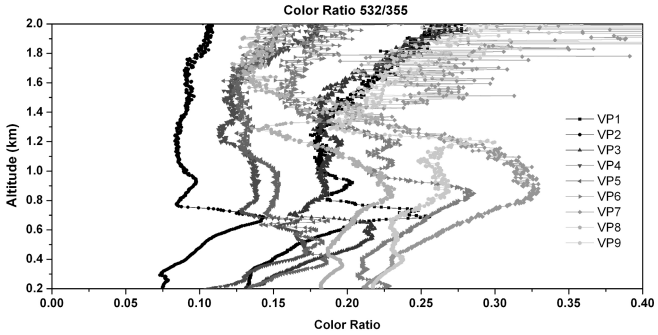

(c)

Figure 6 - Altitude vs Color Ratio: (a) 1064/532 nm; (b) 1064/355nm; (c) 532/355 nm.

Figure 7 shows the concentration of particulate PM_{10} and $PM_{2.5}$ measured at the air quality monitoring station for 24 hours for May 25th 10:00 to 26th 10:00. The concentration of PM_{10} is higher than $PM_{2.5}$, mainly between 10:00 and about 18:00 on May 25th, when it is almost twice as high. This is the time in Figures 2 to 4 that corresponds to the higher signal intensity, indicating a greater mass volume.

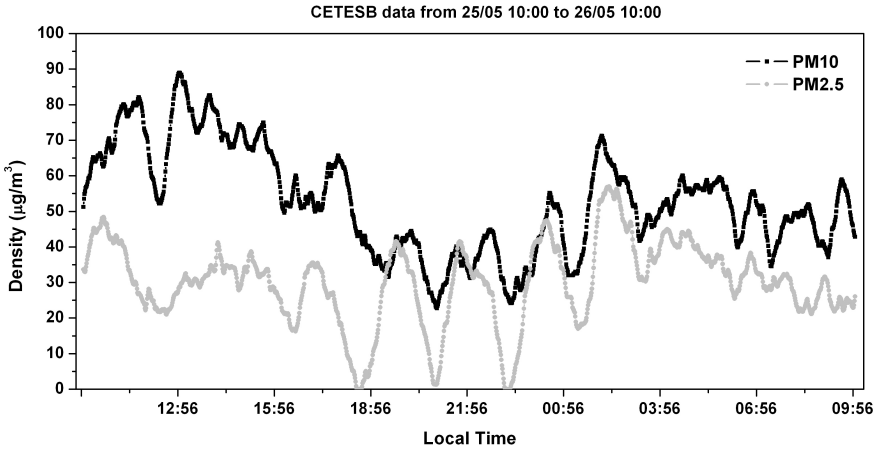

Figure 7 - Concentration of PM_{10} and $PM_{2.5}$ from 10:00 on 25th to May 26th, 2011.

The Sodar observations showed extremely light winds between 10:00 and 22:00, mostly between 1 and 2,5 $m.s^{-1}$, and with the direction widely fluctuating between east and south-southwest, probably not being very significant, due to being within the instrumentation threshold. This might also be the reason for the relatively low vertical range of the measurements up to only 200-250 m AGL. No influence of a sea-breeze circulation was observed at the site on 25 May 2011. From about 22:00 onwards, north-northwesterly winds began to flow from the interior across the escarpment, which ranges from 750-800 m amsl to the northwest of the site, to 850-930 m amsl to the north. From 23:30 to 04:30, wind directions above 200m AGL were from the north, thereafter backing to northwesterly and gradually penetrating down to about 150m by 08:00.

As the surface temperature began to drop in the late afternoon, and also due to the very low wind speeds, a temperature inversion began to gradually develop from 18:30 onwards. It reached its greatest depth and intensity at 21:30, with a temperature increase of 1,5°C from 40m to ±60m (Figure 8a). Thereafter, it gradually dropped in height and began to erode, as the air flow from the interior intensified (Figure 8b), until it totally dissipated by 01:00, due to the katabatic warming of the descending northerly airflow.

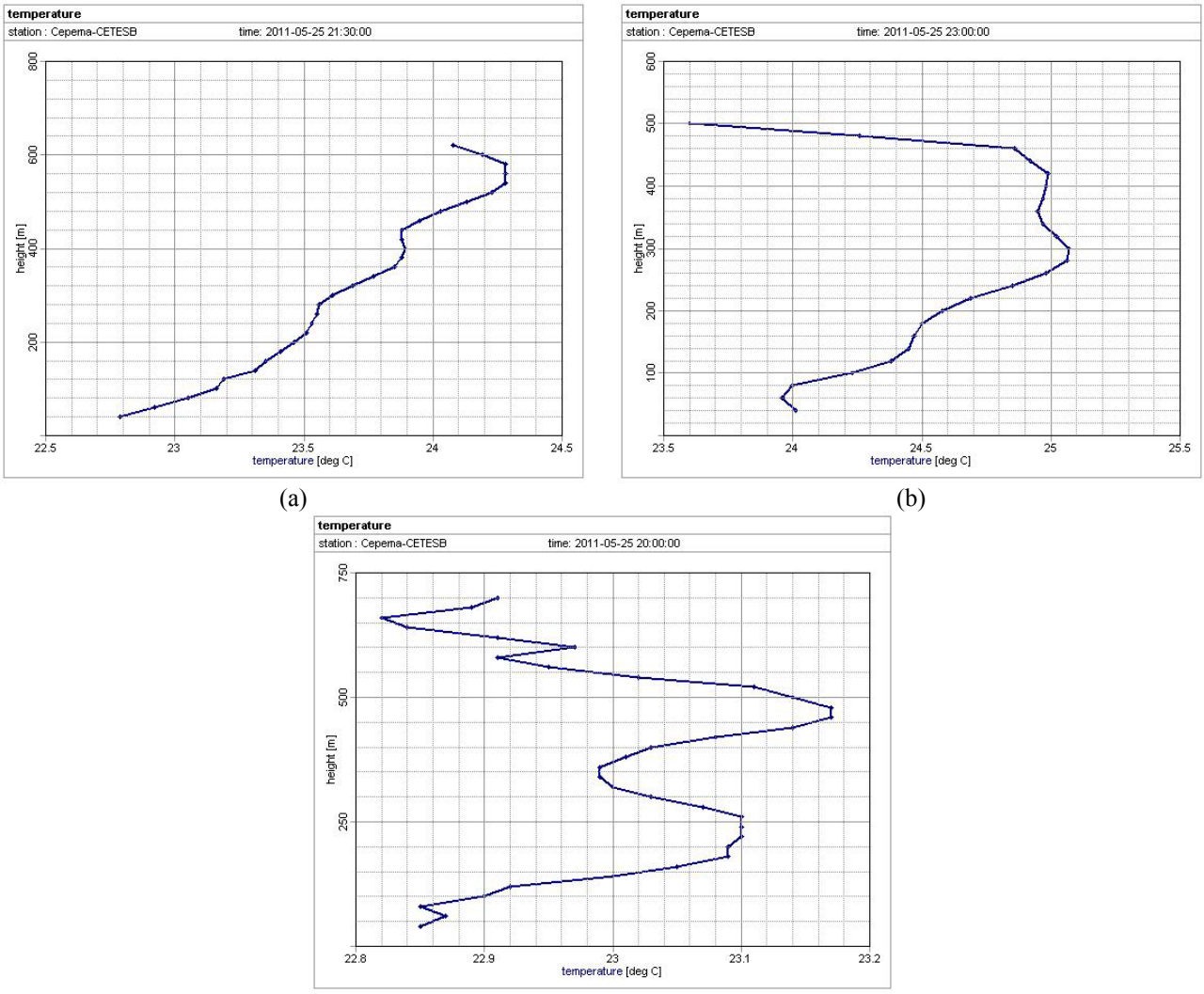

Figure 8 – Vertical profiles of the temperature on 25 May 2011. a) 21:30 (vertical scale up to 800m AGL); b) 23:00 (vertical scale up to 600m AGL); c) 20:00 (vertical scale up to 750m AGL).

It is noteworthy, that due to the complex orography around the monitoring site and the interaction between the large-scale drainage from the interior across the Serra do Mar range and the northeasterly local drainage flow from the industrial area (Fig. 1), created a layered structure of the temperature inversion (Fig. 8c). This ultimately results in several layers of aerosols.

The inversion resulted in an inhibition of vertical mixing in the atmosphere, gradually limiting the aerosol layer from about 850m AGL at 17:00 down to about 500m AGL after 19:00. As the winds backed to northwesterly and became stronger, the aerosols were more widely dispersed and impacted less on the observation site (Figures 2-4).

4. CONCLUSIONS

Observations made from May 25th , 10:00 to May 26th , 10:00, 2011, during a field campaign in Cubatão, using a Lidar with three different wavelengths system, a Sodar with RASS and an air quality monitoring station in order to record the

vertical profile of the atmosphere. Through the coordinated deployment of the three equipments it is possible to interpret what has happened in the atmosphere during the campaign.

Acknowledgments

The authors thank the supporting agencies FAPESP, CNPq, CAPES, Cepema and PETROBRÁS for providing funding for the realization of the field campaign and research.

REFERENCES

[1] Weibring, P.; Abrahamsson, C.; Sjöhlm, M.; Smith, J.N.; Edner, H.; Svamberg, S. Multi-component chemical analysis of gas mixtures using a continuously tunable Lidar system, Applied Physics B, 79, 525-530, 2004.

[2] Agroskin, V.Y.; Bravy, B.G.; Chernyshev, Y.A.; Kashtanov, S.A.; Kirianov, V.I.; Makarov, E.F.; Papin, V.G.; Sotnichenko, S.A.; Vasiliev, G.K. Aerosol sounding with Lidar system based on a DF laser, Applied Physics B, 81, 1149-1154, 2005.

[3] Pappayanis, A. and Balis, D. Study of the structure of the lower troposphere over Athens using backscattering Lidar durig the medcapot-trace experiment:measurements over a suburban area, Atmospheric Environment, Vol. 32, n 12, 2161-2172, 1998.

[4] Chudzynsky, S; Czyzewski, A.; Ernst, K.; Karasinski, G.; Kolacz, K; Pietruczuk, A.; Skubiszak, W.; Stacewicz, T.; Stelmaszczyk, K.; Szymanski, A. Multiwavelenght Lidar for measurement of atmospheric aerosol, Optics and Lasers in Engineering, 37, 91-99, 2002.

[5] Jaques, P.A. and Kim, C.S. Measurement of total lung deposition of inhaled ultrafine particles in healthy men and women. Inhalation Toxicology, vol 12, n8, 715-731, 2000.

[6] Abbas, M.Z.M.; Bruns, R.E.; Scarminio, I.S.; Ferreira, J.R. A multivariate statistical analysis of the composition of rainwater near Cubatão, SP, Brazil, Environmental Pollution, 79, 225-233, 1993.

[7] CETESB (Companhia de Tecnologia e Saneamento Ambiental), "Relatório Anual da Qualidade do Ar no Estado de São Paulo-1992", CETESB, São Paulo, (2003).

[8] Argall, P. S. and Sica, R.J. LIDAR | Atmospheric Sounding Introduction, In: James R. Holton, Editor(s)-in-Chief, Encyclopedia of Atmospheric Sciences, Academic Press, Oxford, 2003, Pages 1169-1176.

[9] Keder, J.; Strizik, M.; Berger, P.; Cerny, A.; Engst, P.; Nemcova, I. Remote sensing detection of atmospheric pollutants by differential absortion LIDAR 510M/SODAR PA2 mobile system, Meteorological Atmospheric Physics, 85, 155-164, 2004.

[10] http://www.sodar.com/about_sodar.htm

[11] http://www.scintec.com/PDFs/Lay_RASS.pdf

[12] Rapoport,V.O.; Fedoseev, Yu. G.; Belova ,N. I.; Sazonov, Yu. A.; Zinichev, V. A. Operating decameter RASS near Nishny Novgorod and perspectives for far radio-acoustic sounding using the Sura HF-radar, Journal of Atmospheric and Terrestrial Physics, 58, (8-9), June-July,1033-1037, 1996.

[13] D. N. Whiteman, B. Demoz, P. Di Girolamo, J. Comer, I. Veselovskii, K. Evans, Z. Wang, M. Cadirola, K. Rush,

G. Schwemmer, B. Gentry, S. H. Melfi, B. Mielke, D. Venable, and T. Van Hove. Raman Lidar Measurements during the International H2O Project. Part I: Instrumentation and Analysis Techniques, Journal of Atmospheric and Oceanic Technology, 23, 157-169, 2006.

[14] B. de Foy, S. P. Burton, R. A. Ferrare, C. A. Hostetler, J. W. Hair, C. Wiedinmyer, and L. T. Molina. Aerosol plume transport and transformation in high spectral resolution lidar measurements and WRF-Flexpart simulations during the MILAGRO Field Campaign. Atmos. Chem. Phys., 11, 3543–3563, 2011.